



Research paper

Numerical simulations of the ONRT ship maneuvering in calm water and head waves with the partially rotating grid method

Sanijo Đurasević^{a,*}, Inno Gatin^b, Hrvoje Jasak^c

^a University of Zagreb, Zagreb, Croatia

^b Cloud Towing Tank, In Silico d.o.o., Zagreb, Croatia

^c University of Cambridge, Cambridge, United Kingdom

ARTICLE INFO

Keywords:

Partially rotating grid method

Actuator disc

Dynamic overset grid

ONRT

Maneuvering

Computational Fluid Dynamics (CFD)

ABSTRACT

This research delves into the maneuverability aspects of a model-scale ONRT surface combatant ship using Computational Fluid Dynamics (CFD) simulations. A key aspect of this study is the comparison of the actuator disc (AD) model and the partially rotating grid (P) method in calm water, complemented by an in-depth analysis of the P method for simulations in waves. Utilizing these methods, the study investigates the performance of the ship in propeller open water, self-propulsion, and complex maneuvers like turning circle and zig-zag. Key findings highlight the superiority of the P method in closely aligning with experimental data, particularly in capturing complex dynamics of ship maneuvers. This research underscores the critical role of propeller side force in maneuvering simulations, a factor often neglected in simpler models like the AD. Maneuvers in head waves are also examined, revealing the nuanced effects of wave orientation on the stability and maneuverability of the ship. This study highlights the effectiveness of CFD in simulating ship maneuvers and the need for ongoing refinement of these techniques to improve accuracy and reliability.

1. Introduction

The shipping industry is currently facing significant challenges in balancing environmental sustainability with operational efficiency. Central to this transformation are the International Maritime Organizations (IMO) stringent regulations, which aim to reduce the environmental impact of maritime operations, particularly focusing on reducing greenhouse gas emissions and enhancing energy efficiency. A key aspect of these regulations is the Energy Efficiency Design Index (EEDI) (IMO, 2014), mandating specific energy efficiency levels for new ship's and underscoring the commitment of the industry to environmentally sustainable practices. Alongside environmental regulations, the IMO also sets standards for ship maneuverability (IMO, 2002), stipulating minimum requirements and assessing crucial aspects like course keeping and turning ability.

The implementation of EEDI criteria significantly influences ship design and performance, highlighting the importance of estimating ship maneuverability in the design phase. This is crucial as adherence to EEDI standards can directly affect a maneuvering capabilities and operational safety of the ship. Additionally, ship maneuverability, especially under varying environmental conditions like wave presence, remains a critical factor for navigational safety. The complexity in assessing

ship maneuverability is heightened by intricate hydrodynamic interactions in different water conditions. As the industry navigates these evolving challenges, the significance of advanced methodologies, particularly Computational Fluid Dynamics (CFD), becomes increasingly recognized.

To assist in designing ship's with optimal maneuvering capabilities, it is crucial to predict how different design choices will impact a maneuverability of the ship. This necessity amplifies the demand for high-fidelity CFD simulations in naval hydrodynamics. There has been a recent surge in CFD studies aimed at assessing and enhancing ship maneuvering performance. Carrica et al. (2013) focus on Unsteady Reynolds Averaged Navier–Stokes (URANS) computations for standard maneuvers of a surface combatant at both model and full scale. Their research highlights the effectiveness of CFD simulations in replicating complex maneuvers like steady turns and zig-zag, achieving highly satisfactory predictions with differences mostly within 10% compared to experimental data. The study also delves into the impact of waves on maneuvers and the complexities involved in modeling propellers. Mofidi and Carrica (2014) conducted CFD simulations of modified and standard zig-zag maneuvers for the KRISO Container Ship (KCS) with a semi-balanced horn rudder and propeller. Despite demonstrating the feasibility of using CFD for such complex maneuvers, they highlighted

* Corresponding author.

E-mail addresses: sdurasevic@fsb.hr (S. Đurasević), inno.gatin@cloudtowingtank.com (I. Gatin), hj348@cam.ac.uk (H. Jasak).

<https://doi.org/10.1016/j.oceaneng.2024.119056>

Received 22 December 2023; Received in revised form 19 August 2024; Accepted 21 August 2024

Available online 31 August 2024

0029-8018/© 2024 Elsevier Ltd. All rights are reserved, including those for text and data mining, AI training, and similar technologies.

Nomenclature

β_s	Steady-state drift angle
β_{\max}	Maximum drift angle during overshoot
ω_R	Angular velocity vector of non-inertial system
c	Adjusted convective velocity
g	Gravitational acceleration vector
u	Absolute velocity field
u_R	Relative velocity field
x	Positional vector
$\delta(t)$	Rudder angle as a function of time
$\delta\theta$	Rotational increment of the propeller per time step
Δt	Time step
Δ	Displacement
η_O	Open water efficiency
λ	Wavelength
λ_z	Length of the relaxation zone
$\mathcal{R}(\phi)$	Relaxation zone operator
$\mathcal{T}(\phi)$	General transport operator acting on the field ϕ
ν	Kinematic viscosity
ν_e	Effective kinematic viscosity
ϕ_s	Steady-state roll angle
ϕ_{\max}	Maximum roll angle
ϕ_{\min}	Minimum roll angle
ψ	Level set function
$\Psi(t)$	Current yaw angle
Ψ_C	Target yaw angle
ρ	Density field
θ	Trim
ε	Propeller shaft angle
ε_w	Width parameter
A_θ	Coefficient for tangential velocity jump
A_x	Coefficient for pressure jump boundary condition
AD	Advance
B	Waterline beam
b	Diffusion coefficient
D	Propeller diameter
d	Shortest distance to the boundary
Fr	Froude number
H	Wave height
J	Advance ratio
K_Q	Torque coefficient
K_T	Thrust coefficient
k_{xx}	Roll radius of gyration
k_{yy}	Pitch radius of gyration
k_{zz}	Yaw radius of gyration
L	Length of waterline
LCB	Longitudinal center of buoyancy (aft of forward perpendicular)
n	Rate of propeller rotation
n_I	Inertial propeller rotation rate
n_R	Non-inertial propeller rotation rate
P	Proportional controller
p	Pressure field
p_d	Dynamic pressure field

p_s	Spatial exponent
PI	Proportional Integral controller
Q	Torque
R	Propeller radius
r^*	Normalized disc radius
r_s	Steady-state yaw rate
r_H	Propeller hub radius
r_{\max}	Maximum yaw rate during overshoot
T	Thrust
T_d	Draft
T_{180}	Time to change heading by 180 degrees
T_{360}	Time to change heading by 360 degrees
T_{90}	Time to change heading by 90 degrees
TD	Tactical diameter
TR	Transfer
U_0	Initial approach speed
V_s	Steady forward velocity
VCG	Vertical center of gravity
w	Weight field
x	Global coordinate axis, positive toward the bow
y	Global coordinate axis, positive toward the starboard side
Z	Number of blades
z	Global coordinate axis, positive downward
z_s	Sinkage

significant computational costs, with total process time extending up to four months for new geometries. Their results showed satisfactory alignment with experimental data, particularly in motion rates and propeller dynamics. However, the study noted a need for improved rudder flow modeling, as CFD predictions differed from experimental observations in terms of absolute speed changes during maneuvers, underscoring the complexity of accurately simulating rudder flow and its turbulence characteristics. Broglia et al. (2015) conducted an in-depth study on the maneuvering of a twin-screw single-rudder vessel using a URANS solver. They observed high drift angles during maneuvers due to the vessels poor course-keeping qualities, which presented a challenge in terms of flow field complexity, involving intense vortical structures and large separation regions. Despite these challenges, their simulations showed good agreement with free-running model tests, with prediction errors under 10%. The study emphasized the significant impact of stern appendages and the propulsion system on the vessels dynamics. In particular, they noted the critical role of propeller behavior and its influence on course stability, highlighting the complexities of propeller-rudder interactions and their importance in maneuvering predictions. Building upon Broglia et al. work (Broglia et al., 2015; Dubbio et al., 2016) extended the analysis to a twin rudder configuration, comparing it with the single rudder model. Their CFD simulations reveal the complex interactions between rudder and propeller, highlighting the significance of stern appendages in maneuvering behavior, especially in multi-screw vessels. Wang et al. (2018) focused on the Office of Naval Research Tumblehome (ONRT) surface combatant ship model, conducting CFD simulations for zig-zag maneuvers in various wave conditions. They demonstrated the feasibility and reliability of using CFD methods to simulate ship maneuvers in waves, noting significant wave-induced motions and unsteady hydrodynamic loads. In their study, Guo et al. (2018) explored hull-propeller-rudder interactions in twin-screw ship's using CFD. They emphasized the importance of propeller side force and asymmetric flow-straightening effects on maneuverability and validated their CFD-based modeling approach against experimental data, providing insights

into the complex interactions during maneuvers. Jin et al. (2019) utilized URANS computations to study self-propelled turning circle and zig-zag maneuvers, comparing different propeller modeling methods. They highlighted the advantages and limitations of each method, showing that while the body-force method is computationally less demanding, the discretized propeller model provides higher fidelity in flow physics near the propeller and rudder regions. Wang and Wan (2020) investigated the stopping ability of the ship through CFD simulations of various maneuvers, including stopping with reversing propeller and turning rudder. Kim et al. (2021a) estimated the maneuverability of the KRISO Very Large Crude Carrier (KVLCC2) ship using CFD with rigid body motion and body force propeller method. Their study demonstrates better agreement of CFD-based free running simulation with model tests compared to system-based methods, highlighting the effectiveness of CFD in predicting ship maneuverability. Shang et al. (2021) conducted systematic CFD simulations of turning circle and zig-zag maneuvers for an S175 boat, using dynamic overset grid and body-force methods with a double-body model to represent the free surface. Their results show satisfactory agreement with experimental data, indicating the applicability of these methods in predicting ship maneuvering characteristics. In their comprehensive study, Kim et al. (2021c) developed and validated direct CFD models to assess the maneuvering performance of a KCS in various wave conditions. Utilizing advanced simulation techniques, including a dynamic overset grid method and a commercial RANS solver, their study focused on the impact of different wave directions on the ship maneuverability. The simulations, validated against experimental data, demonstrated reliability of CFD in predicting key maneuvering parameters like advance, transfer, and tactical diameter with minimal uncertainty. This research underscores the significance of wave conditions in ship maneuvering. Kim et al. (2021b) further explore the effects of wavelength on ship maneuverability using CFD. Their research reveals that wavelength significantly influences approach speeds, ship motions, and maneuvering parameters, enhancing the understanding of ship maneuverability in waves. Recently, Aram and Mucha (2023) performed a detailed CFD analysis to compare a virtual disc model with a discretized propeller model for ship maneuvering simulations. Focusing on the ONRT surface combatant, their study revealed that the discretized propeller model provided more accurate maneuvering predictions than the body force model, particularly due to its ability to account for propeller side forces. This research highlights the importance of choosing the right propeller model for precise maneuvering analysis in calm water conditions.

The comprehensive studies presented in this overview underscore the progressive advancements and critical importance of high-fidelity CFD in naval hydrodynamics, particularly in estimating ship maneuverability. They collectively reveal a multifaceted picture: while CFD offers the potential for precise simulation and prediction of complex maritime maneuvers, it also brings to light the challenges in computational demands and the need for improved modeling techniques, especially in the area of propeller modeling.

Addressing the challenge of significant time scale differences in flow phenomena near the hull and propeller in maneuvering simulations, Carrica et al. (2015) introduced a novel method involving a local, partially rotating frame within the dynamic overset grids that define the propeller. This technique decouples the propeller grid rotation from the actual propeller rotation within each time step. Consequently, the propeller blades traverse the wake over a longer duration than in real-time rotation. However, given the rapid rotation of the propeller relative to the duration of the maneuver, this method still effectively approximates the average forces necessary for accurate maneuver resolution. Building upon this concept, Đurasević et al. (2022) implemented a partially rotating grid method within the Naval Hydro Pack (Vukčević et al., 2017) library, which utilizes the foam-extend (Weller et al., 1998) software. The focus of the work was upon assessing the accuracy of this method for a self-propelled KCS ship at both model and full-scale. Subsequently, the research was expanded in Đurasević et al.

(2023), extending the application to a two-phase solver. This extension focused on investigating the accuracy of the method in predicting the hydrodynamic performance of full-scale ship equipped with a Pre-Swirl Duct (PSD).

This study represents a continuation in the line of research on the partially rotating grid (P) method by extending it to assess turning circle and zig-zag maneuvers of a model-scale ONRT surface combatant. In calm water conditions, our focus includes a detailed comparison between the P method and the actuator disc (AD) model. This comparison primarily evaluates critical maneuvering parameters, such as ship velocities, trajectories, ship motions, and correlates them with publicly available experimental data (EFD) (Sanada et al., 2019; Elshiekh, 2014). The study then extends to exclusively apply the partially rotating grid method for analyzing turning circle and zig-zag maneuvers in head waves.

The structure of this paper is organized as follows: Section 2 details the numerical model and the governing equations crucial to this study. Section 3 provides a comprehensive description of the geometry of the ship used in our research, accompanied by an in-depth explanation of the setup for various simulations, including propeller open water, self-propulsion, and maneuvering. The findings from these simulations are extensively analyzed and discussed in Section 4. The paper concludes with Section 5, summarizing the key findings and implications of this study.

2. Numerical model

The equations utilized in this study are integrated into the Naval Hydro Pack (Vukčević et al., 2017) library, which enhances the foam-extend (Weller et al., 1998) capabilities for naval hydrodynamics CFD applications. Continuity equation for viscous incompressible flow is defined as:

$$\nabla \cdot \mathbf{u} = 0, \quad (1)$$

where \mathbf{u} is absolute velocity field. Single-phase momentum equation derived in the relative frame with absolute velocity is employed for propeller open water simulation:

$$\frac{\partial \mathbf{u}}{\partial t} + \nabla \cdot (\mathbf{u}_R \mathbf{u}) = -\frac{\nabla p}{\rho} + \nabla \cdot (\nu \nabla \mathbf{u}) - \boldsymbol{\omega}_R \times \mathbf{u}, \quad (2)$$

where \mathbf{u}_R is relative velocity field, p is a pressure field, ρ is a density field, ν is kinematic viscosity, and $\boldsymbol{\omega}_R$ is angular velocity vector.

In the context of viscous, two-phase incompressible flows, the momentum equation, when formulated in the inertial frame and considering absolute velocity, is expressed as:

$$\frac{\partial \mathbf{u}}{\partial t} + \nabla \cdot (\mathbf{u} \mathbf{u}) = -\frac{\nabla p_d}{\rho} + \nabla \cdot (\nu_e \nabla \mathbf{u}), \quad (3)$$

In this equation, ρ signifies a field of discontinuous density, while ν_e represents the effective kinematic viscosity, comprising both the kinematic and turbulent kinematic viscosities. Additionally, the dynamic pressure field, denoted as p_d , is defined by the equation:

$$p_d = p - \rho \mathbf{g} \cdot \mathbf{x}. \quad (4)$$

Here, \mathbf{g} is identified as the gravitational acceleration vector, and \mathbf{x} as the positional vector. In this study, we apply this formulation of the momentum equation (Eq. (3)) in the inertial frame specifically for maneuvering simulations using the AD model.

For maneuvering simulations employing the P method, the momentum equation is adapted for the relative frame while utilizing absolute velocity:

$$\frac{\partial \mathbf{u}}{\partial t} + \nabla \cdot (\mathbf{u}_R \mathbf{u}) = -\frac{\nabla p_d}{\rho} + \nabla \cdot (\nu_e \nabla \mathbf{u}) - \boldsymbol{\omega}_R \times \mathbf{u}. \quad (5)$$

This method incorporates a dual representation of propeller rotation, blending both non-inertial and inertial components. Here, the total angular velocity vector $\boldsymbol{\omega}$ comprises the sum of the angular velocity

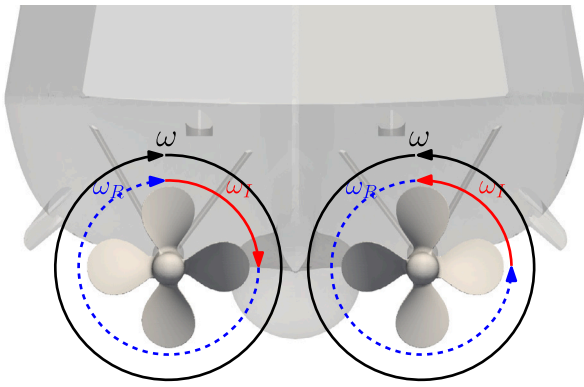


Fig. 1. Graphical representation of the ω components.

of the rotating appendage grid ω_I and the non-inertial systems angular velocity ω_R as graphically presented in Fig. 1. The rate of propeller rotation, n , is thus a composite of an inertial part (n_I) and a non-inertial part. The inertial aspect of the propeller (ω_I) influences the overall duration of the simulation, whereas the non-inertial component (ω_R) introduces a rotational effect through an additional source term in the momentum equation, not affecting the transient aspect of the equation.

In the current study, the free-surface interface is captured using a conservatively modified implicitly re-distanced Level Set (LS) approach (Vukcevic and Jasak, 2014). This LS method utilizes a signed distance function, where the value denotes the perpendicular distance to the free surface. The governing equation for the LS field, ψ , is formulated as follows (Vukčević et al., 2016a,b):

$$\frac{\partial \psi}{\partial t} + \nabla \cdot (\mathbf{c}\psi) - \psi \nabla \cdot \psi - b \nabla \cdot (\nabla \psi) = b \frac{\sqrt{2}}{\varepsilon_w} \tanh \frac{\psi}{\varepsilon_w \sqrt{2}}, \quad (6)$$

In this equation, the variables b and ε_w represent the diffusion coefficient and the width parameter, respectively, while \mathbf{c} signifies the adjusted convective velocity. This formulation enhances the accuracy and conservation properties of the LS method, making it well-suited for the complex hydrodynamic simulations presented in this work.

To ensure the applicability of Eqs. (1), (3), and (5) across the fluid interface, it is essential to incorporate jump conditions that address the discontinuity in the density field. The Ghost Fluid Method (GFM) is utilized for this purpose, offering interface-corrected discretization schemes for various mathematical operators (Vukčević et al., 2017).

To accurately simulate the motion of a ship, the solution algorithm incorporates equations for 6-DOF (Degrees of Freedom) rigid body motion (Gatin et al., 2017). These equations enable the calculation of forces exerted on a floating body within a global Cartesian coordinate system. These forces are subsequently transformed to align with a body-fixed coordinate system. This process forms a set of ordinary differential equations. Solving these equations provides insights into the displacement and velocity of the floating body. Consequently, the computational grid is adapted and moved in tandem with the displacement of the body, ensuring a coherent and dynamic representation of the ship's movement within the simulation environment.

The closure of the governing equations in this study is achieved using the $k-\omega$ Shear Stress Transport (SST) turbulence model (Menter et al., 2003). Time derivatives are discretized using second-order accurate implicit backward scheme. The convection term in the momentum equations (referenced in Eqs. (2), (3), (5)) is discretized applying the Gauss theorem, where linear, upwind-biased interpolation is employed for translating values from cell-centers to face-centers. All diffusion terms follow a discretization approach using the Gauss theorem with central differencing, incorporating an over-relaxed technique for non-orthogonal corrections. The propeller motion in simulations is represented through the dynamic overset grid method (Gatin et al., 2018). To

solve the governing equations, the study adopts the PIMPLE algorithm, a hybrid that combines the strengths of the SIMPLE (Semi-Implicit Method for Pressure-Linked Equations) (Patankar and Spalding, 1972) and PISO (Pressure Implicit with Splitting of Operator) algorithms (Issa, 1986).

The AD model is represented with equations that effectively introduce thrust and torque into the flow, effectively capturing axial and tangential flow accelerations. Key equations in this model include the pressure jump boundary condition and the equation for tangential velocity jump:

$$\Delta p = A_x r^* \sqrt{1 - r^*}, \quad (7)$$

where r^* is a normalized disc radius, and A_x is calculated based on the propellers thrust, radius, and hub radius.

$$\Delta U_\theta = A_\theta \frac{r^* \sqrt{1 - r^*}}{r^*(1 - r'_H) + r'_H}, \quad (8)$$

where $r'_H = r_H/R$, and A_θ is determined by the propellers torque, axial velocity, and geometrical parameters.

In this research, wave modeling is accomplished through the integration of potential flow wave theories with CFD solution (Jasak et al., 2015; Vukčević et al., 2016a). A key technique employed is the use of relaxation zones, designed to seamlessly transition between the simplified wave theory equations and the more complex CFD calculations. Within these relaxation zones, the governing equations of fluid dynamics are volumetrically combined with the incident far-field solutions derived from wave theory. This integration is restricted to the relaxation zones, with pure CFD solutions applied outside these areas. A critical challenge in wave modeling is the effective damping of waves at the wave tanks end. This is necessary to prevent wave reflections from contaminating the study results. The relaxation zones address this by blending the flow models governing equations with prescribed incident far-field solutions. This blending ensures that only the clean incident flow is present near the boundaries, thus preventing wave reflection. The process utilizes a weight field, denoted as w , which serves to merge the two models according to the equation:

$$(1 - w)\mathcal{T}(\phi) + w\mathcal{R}(\phi) = 0 \quad (9)$$

In this equation, $\mathcal{R}(\phi)$ represents the relaxation zone operator, and $\mathcal{T}(\phi)$ signifies the general transport operator acting on the field ϕ . The weight field is configured to have a value of 1 at the far field, gradually decreasing to 0 as it moves towards the interior of the domain. For this study, the weight field is characterized by an exponential function:

$$w = \frac{\exp\left(\frac{d}{\lambda_z}\right)^{p_s} - 1}{e - 1} \quad (10)$$

Here, λ_z is the length of the relaxation zone, d represents the shortest distance to the boundary, and p_s is the spatial exponent.

3. Simulation setup

This study focuses on a model-scale ONRT surface combatant, equipped with two four-bladed propellers, a pair of rudders, a skeg, and bilge keels, as depicted in Fig. 2. The geometry selected for this study represents design of a modern surface combatant, a configuration that is publicly accessible for research purposes. This particular model has been a subject of analysis at the Tokyo 2015 Workshop on CFD in Ship Hydrodynamics (Tokyo, 2015) and is currently a popular choice for validating CFD codes, especially in the realm of maneuvering simulations. Main particulars of the ship are detailed in Table 1. For the purpose of this study, the global coordinate systems origin is placed at the aft perpendicular, aligned with the undisturbed waterline. The orientation of the coordinate axes is defined as follows: the positive x -axis points towards the bow, the positive y -axis extends towards the starboard side, and the positive z -axis is directed downward. The hull



Fig. 2. ONRT surface combatant geometry.

Table 1

Main ship particulars.

Length of waterline	L , m	3.147
Waterline beam	B , m	0.384
Draft	T_d , m	0.112
Displacement	Δ , kg	72.6
Longitudinal center of buoyancy (aft of FP)	LCB , m	1.625
Vertical center of gravity	VCG , m	0.156
Roll radius of gyration	k_{xx}/B , -	0.374
Pitch radius of gyration	k_{yy}/L , -	0.246
Roll radius of gyration	k_{zz}/L , -	0.246
Propeller diameter	D , m	0.1066
Number of blades	Z , -	4
Propeller shaft angle	ϵ_s , °	5

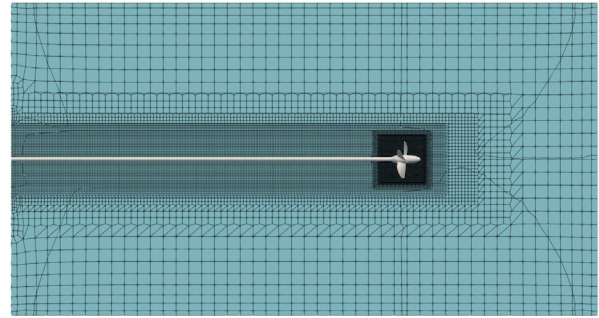
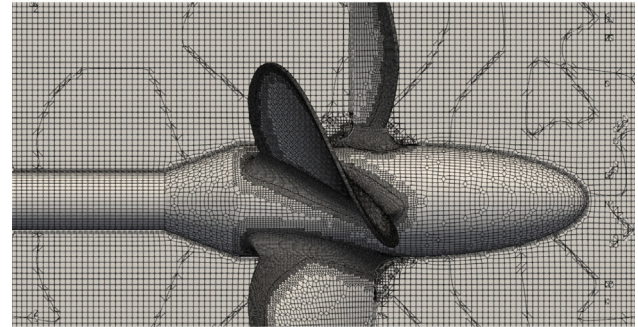
and appendages are presumed to be hydraulically smooth, and the simulations utilize constant thermophysical properties of the water at 20 °C.

Propeller open water simulations are essential in this study for obtaining crucial data needed for self-propulsion and maneuvering analyses using the AD model which utilizes propeller open water data as inputs to compute thrust and torque. The computational setup is organized into two distinct regions: a background grid with a cylindrical shape and a propeller-specific cylindrical region dynamically coupled to the background grid through the overset grid method. These simulations are carried out at model scale. The propellers rotation rate is maintained constant, and the inlet velocity of the computational domain is varied accordingly. The domain outlet is defined with a pressure outlet boundary condition, while a slip condition is applied to the external cylindrical boundary of the background grid. The flow equations are resolved employing the partially rotating grid method, where the inertial propeller rotation rate is set to a fraction ($n_I = 0.1 \cdot n$) of the total rotation rate, and the non-inertial rotation rate comprises the remaining fraction ($n_R = 0.9 \cdot n$). A cross-sectional view of the discretized computational domain is depicted in Fig. 3. The domain dimensions adhere to the ITTC guidelines (ITTC, 2021). The simulations span a range of advance ratios (J), specifically 0.4, 0.6, 0.8, 1.0, and 1.2. The time-step for the simulation is determined using the equation:

$$\Delta t = \frac{\delta\theta}{n_I \cdot 360}, \quad (11)$$

where $\delta\theta = 1^\circ$ represents the rotational increment of the propeller per time step.

In case of self-propelled ship simulations computational domains discretization is structured to maintain specific distances relative to the hull: the inlet is positioned at $2L_{pp}$, the outlet at $2.5L_{pp}$, the sides at $1.5L_{pp}$, the top at $0.5L_{pp}$, and the bottom at $1.5L_{pp}$. Details of the discretized domain are shown in Fig. 4. The grids are primarily composed of hexahedral elements, with the total number of cells being 6.68×10^6 for the AD simulations and 9.81×10^6 for the partially rotating grid simulations. The near-wall flow behavior and boundary layer effects are modeled using the wall functions approach to optimize computational resource usage. The average dimensionless wall distance (y^+) is approximately 37. The grid configuration includes four overset regions (two rudders and a background grid fitted to the ship hull) for AD simulations, and five overset regions (two rudders, two propellers, and a background grid shaped to the ship hull) in the partially rotating grid simulations.

(a) $y = 0$ plane view,

(b) Propeller grid surface mesh,

Fig. 3. Propeller open water simulations grid.

In self-propulsion simulations employing the AD model, axial velocity field at the propeller plane determine the advance speed and ratio. The thrust (K_T) and torque (K_Q) coefficients, essential for calculating thrust and torque, are interpolated from propeller open water data using the established advance ratio. Pressure and velocity jumps are then applied through the actuator disc patch. These simulations, both for the AD and P methods, aim for force equilibrium along the longitudinal axis, adjusting the propeller rotation rate through a Proportional Integral (PI) controller (ITTC, 2021). The proportional (K_P) and integral (K_I) gain constants are computed as described in Đurasević et al. (2022). To maintain the course during self-propulsion, a Proportional (P) controller is used:

$$\delta(t) = K_P(\Psi_C - \Psi(t)), \quad (12)$$

where $\delta(t)$ is the rudder angle, Ψ_C is the target yaw angle set to 0 degrees, and $\Psi(t)$ is the current yaw angle. The proportional gain is fixed at 1. The initiation of turning circle and zig-zag maneuvers in the simulations begins from the self-propulsion solution. For portside turning circle maneuver, the rudder is deflected at a constant rate of $35^\circ/s$ to a maximum angle of 35° and maintained there. In zig-zag maneuver, the rudder is deflected to 20° at the same rate and held until the ship's heading matches the maximum rudder angle. Upon reaching a heading of 20° , the rudder is then deflected to -20° .

Maneuvering simulations in both calm water and waves are conducted at a Froude number $Fr = 0.2$, starting with an initial approach speed $U_0 = 1.11$ m/s. In case of partially rotating grid method, inertial propeller rotation rate is set to $n_I = 0.1 \cdot n$ and the non-inertial rotation rate is set to $n_R = 0.9 \cdot n$. Selecting these values allows for an increased timestep, approaching those suitable for resolving flow near the hull while still maintaining accurate thrust and torque predictions essential for correct maneuvering prediction. The simulation timestep is consistently set for both the AD model and the partially rotating grid method. It is determined using Eq. (11), with a rotational increment $\delta\theta = 1.5^\circ$. The approximate value of Δt thus calculated is approximately 4.7736×10^{-3} s. Consequently, the computational times for both methods

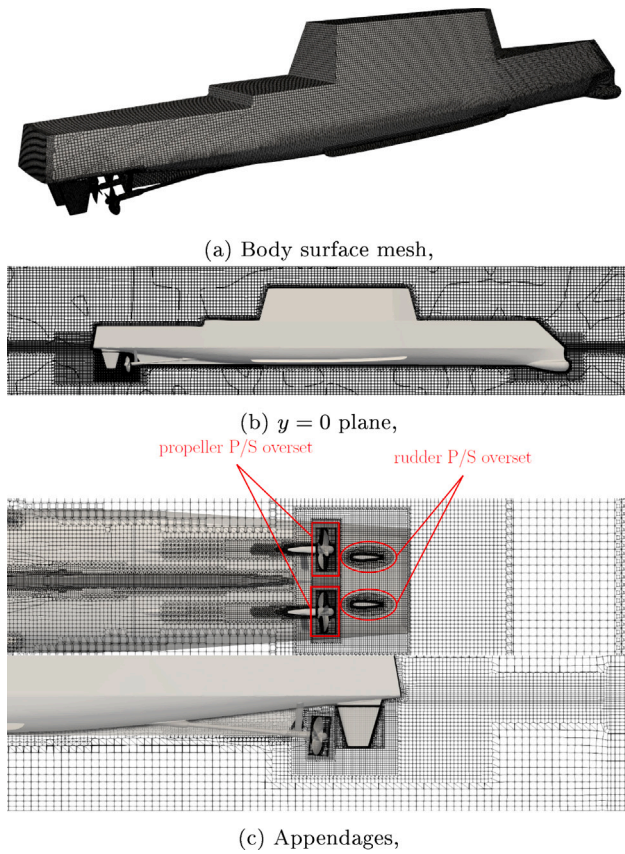


Fig. 4. Grid structure.

are comparable in this scenario, each requiring approximately 4800 core-hours to complete the simulations in case of zig-zag in calm water. It is noteworthy that with a fully inertial propeller rotation representation (where $n_i = n$), the calculated timestep would be approximately 4.7736×10^{-4} s. This value is an order of magnitude smaller compared to the timestep in the case of the P method, where $n_i = 0.1 \cdot n$. To align closely with the experimental setup (Sanada et al., 2019; Elshiekh, 2014), 6-DOF rigid body motion equations are integrated into the simulation process. For the turning circle and zig-zag maneuvering simulations in waves, the chosen parameters are a wavelength $\lambda = L$ and a wave steepness $H/\lambda = 0.02$, where H represents the wave height. Simulations in waves are solely performed using the P method.

4. Results and discussion

The section presents and discusses the results of CFD simulations. Initially, it outlines and analyzes results from the propeller open water simulations, followed by a review of the self-propulsion simulation results. The analysis then progresses to the turning circle and zig-zag 20/20 maneuvers in calm water, comparing these results against EFD data, including an assessment of the AD model and the P method. The section concludes with an examination of the CFD simulations using only the P method for turning circle and zig-zag 20/20 maneuvers in head wave conditions.

4.1. Propeller open water simulations

To acquire the necessary data for the AD model, propeller open water simulations are conducted. The results from these simulations are then compared with the publicly available model-scale propeller data (Tokyo, 2015). The simulations for various advance ratios, as

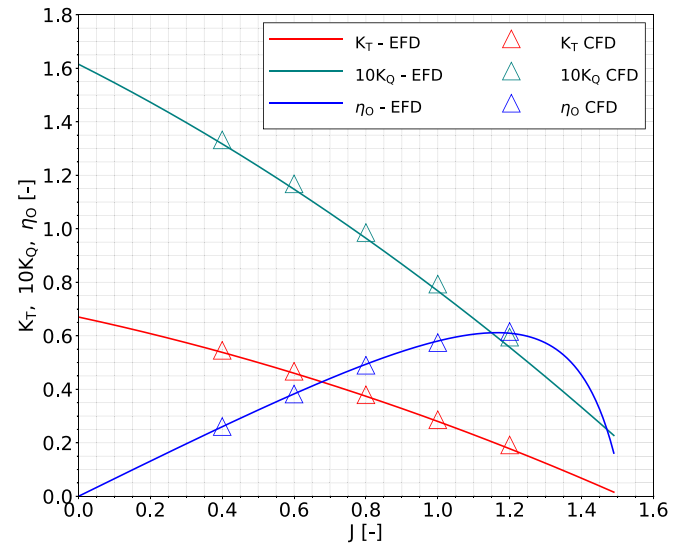


Fig. 5. Propeller open water characteristics.

Table 2

Propeller open water data.

J , –	K_T , –	$10K_Q$, –	η_o , –
0.4	0.5475 (1.06%)	1.3323 (1.13%)	0.2607 (0.68%)
0.6	0.4674 (1.53%)	1.1679 (1.62%)	0.3822 (–0.01%)
0.8	0.3794 (1.42%)	0.9859 (2.21%)	0.4899 (–0.75%)
1.0	0.2864 (2.03%)	0.7931 (3.22%)	0.5746 (–1.11%)
1.2	0.1919 (7.84%)	0.5949 (6.56%)	0.6161 (1.02%)

detailed in Section 3, are executed using the partially rotating grid method. The thrust (T) and torque (Q) of the propeller are determined by integrating the pressure and viscous forces across the propellers surface. These values enabled the calculation of the thrust coefficient ($K_T = T/(\rho_w n^2 D^4)$), torque coefficient ($K_Q = Q/(\rho_w n^2 D^5)$), and open water efficiency ($\eta_o = (JK_T)/(2\pi K_Q)$). The results are illustrated in Fig. 5, where the EFD data are represented by solid lines and the CFD data by markers. Table 2 enumerates the numerical CFD values along with their relative differences when compared to experimental data ($E_r, \%EFD = (CFD - EFD)/(EFD) \times 10^2$) for each specified advance ratio.

In this study, we observe an overestimation in CFD simulation results for thrust and torque coefficients compared to model-scale experimental data, particularly at higher advance ratios (see Fig. 5 and Table 2). This overestimation in the model-scale CFD simulations could be attributed to several factors unique to the model-scale testing environment. At the model scale, flow around the propeller often experiences laminar conditions, transitional flows, and more pronounced flow separations compared to typical full-scale turbulent conditions. These specific flow characteristics at the model scale, particularly the presence of laminar flow and enhanced flow separation, can lead to larger simulated values of thrust and torque coefficients. This is because laminar flows are less efficient at transferring momentum and increased separation can elevate force estimations in simulations. The observed discrepancies in thrust and torque coefficients between CFD simulations and model-scale experimental data suggest two potential courses of action for improved alignment with experimental observations. Firstly, model-scale CFD simulations might benefit from further calibration or adjustments to more accurately capture the unique flow phenomena prevalent at this scale, such as laminar flow and increased flow separation. Secondly, the introduction of turbulators in the model

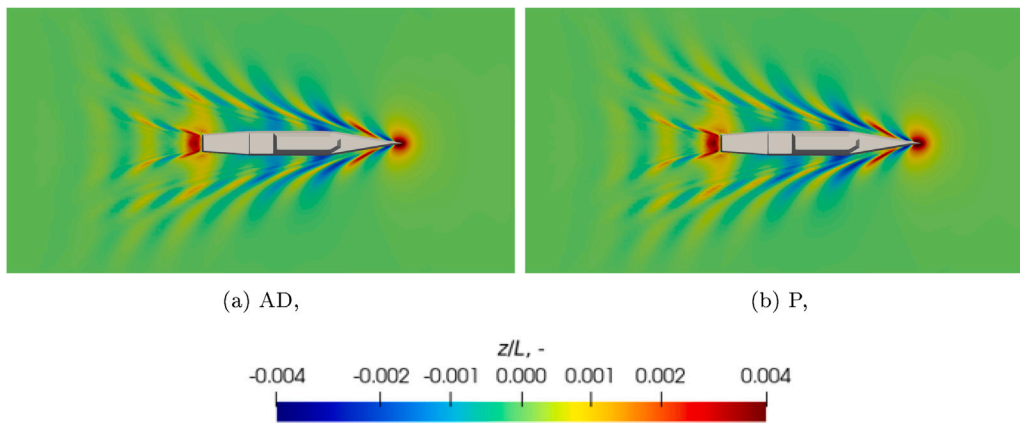


Fig. 6. Free surface elevation (calm water).

Table 3

Self-propulsion data.

	n , s^{-1}	z_s , $\times 10^{-2}$ m	θ , $^\circ$
EFD	8.97	0.2262	-0.0386
AD	8.69	0.1606	-0.0602
	(-3.12%)	(-29.0%)	(55.96%)
P	8.75	0.1786	-0.0459
	(-2.45%)	(-21.04%)	(18.91%)

testing setup could be considered to induce a fully turbulent flow. For the current scope of this study, the relative differences observed are considered to be acceptable.

4.2. Self-propulsion

The self-propulsion point, set at an approach speed of 1.11 m/s, is reached at a propeller rotation rate of 8.69 s^{-1} in the AD simulation and 8.75 s^{-1} in the P simulation. Upon comparing these values with the EFD data, relative differences of -3.12% and -2.45% are observed for the AD and P simulations, respectively (see Table 3). These findings indicate a slight underestimation of the propeller rotation rate compared to the model test. However, they also affirm the effectiveness of both the AD and P methods in executing self-propulsion simulations with reasonable accuracy. The free surface generated in both the AD and P simulations is visually represented in Fig. 6. In analyzing the discrepancies between the CFD simulations and experimental data for sinkage and trim, it is crucial to consider the impact of the small absolute values involved. The experimental data for sinkage and trim, recorded as 0.2262 m and -0.0386 degrees respectively, are quite modest. This factor plays a significant role in the interpretation of the relative differences observed in the CFD results. For instance, the AD simulation shows a sinkage of 0.1606 m and a trim of -0.0602 degrees, resulting in relative differences of -29.0% and 55.96% compared to the experimental values. Similarly, the P simulation indicates a sinkage of 0.1786 m and a trim of -0.0459 degrees, corresponding to relative differences of -21.04% and 18.91%. These percentages, while seemingly large, are primarily a consequence of the small base values in the experimental data. Therefore, the observed discrepancies in percentages are more indicative of a mathematical characteristic of the relative difference calculation rather than substantial physical variations in the CFD models. Such nuances are essential to acknowledge when interpreting CFD results, especially in cases where the absolute values are small.

4.3. Turning circle maneuver in calm water

The converged state from the self-propulsion simulation is used as the initial state for the turning circle maneuver simulation towards the

Table 4

Turning circle calm water parameters.

	EFD	AD	P
Advance, AD/L , -	2.329	2.278 (-2.19%)	2.320 (-0.39%)
Tactical, TD/L , -	3.174	3.082 (-2.90%)	3.174 (0.03%)
Transfer, TR/L , -	1.288	1.239 (-3.80%)	1.258 (-2.31%)
Steady, D/L , -	3.188	3.038 (-4.73%)	3.082 (-3.32%)
$T_{90}V_0/L$, -	3.734	3.603 (-3.51%)	3.774 (1.07%)
$T_{180}V_0/L$, -	7.602	7.204 (-5.28%)	7.777 (2.3%)
$T_{360}V_0/L$, -	15.496	14.147 (-8.71%)	15.324 (-1.11%)
V_s/V_0 , -	0.637	0.656 (2.98%)	0.631 (-0.95%)
r'_s , -	-0.689	-0.679 (-1.45%)	-0.660 (-4.31%)
β_s , $^\circ$	11.763	13.368 (13.64%)	12.967 (10.23%)
ϕ_{min} , $^\circ$	-2.404	-2.432 (1.16%)	-2.163 (-10.01%)
ϕ_{max} , $^\circ$	4.852	4.291 (-11.56%)	4.754 (-2.03%)
ϕ_s , $^\circ$	2.235	2.396 (7.20%)	2.493 (11.53%)

portside. The propeller rotation rate for both the AD and P methods is set to a fixed value, as obtained from the self-propulsion simulation, as described in Section 4.2. The comparative analysis of the portside turning circle maneuvering data involves comparing the performances of the AD and P simulations against the EFD data. Obtained values are summarized in Table 4.

The AD and P simulations exhibit minor variations in the advance (AD/L), with the P method showing a closer alignment to the EFD data. The tactical diameter (TD/L), a critical measure of the ship's turning capability, is replicated very well by the P simulation, contrasting with the AD method's slight underestimation. Both simulations exhibit underestimations in the transfer (TR/L), with the P simulation once again demonstrating a closer alignment with the experimental values. The value of the steady turning diameter (D/L) is underestimated by both methods compared to the experimental data, with the P method being more accurate. Various time to change heading parameters ($T_{90}V_0/L$, $T_{180}V_0/L$, $T_{360}V_0/L$) further illustrate the disparity between the two simulation methods. The AD method consistently underestimates these values, while the P method shows a mix of under and overestimation, reflecting its varying degrees of accuracy in different aspects of the maneuver. In terms of ship's forward velocity in steady

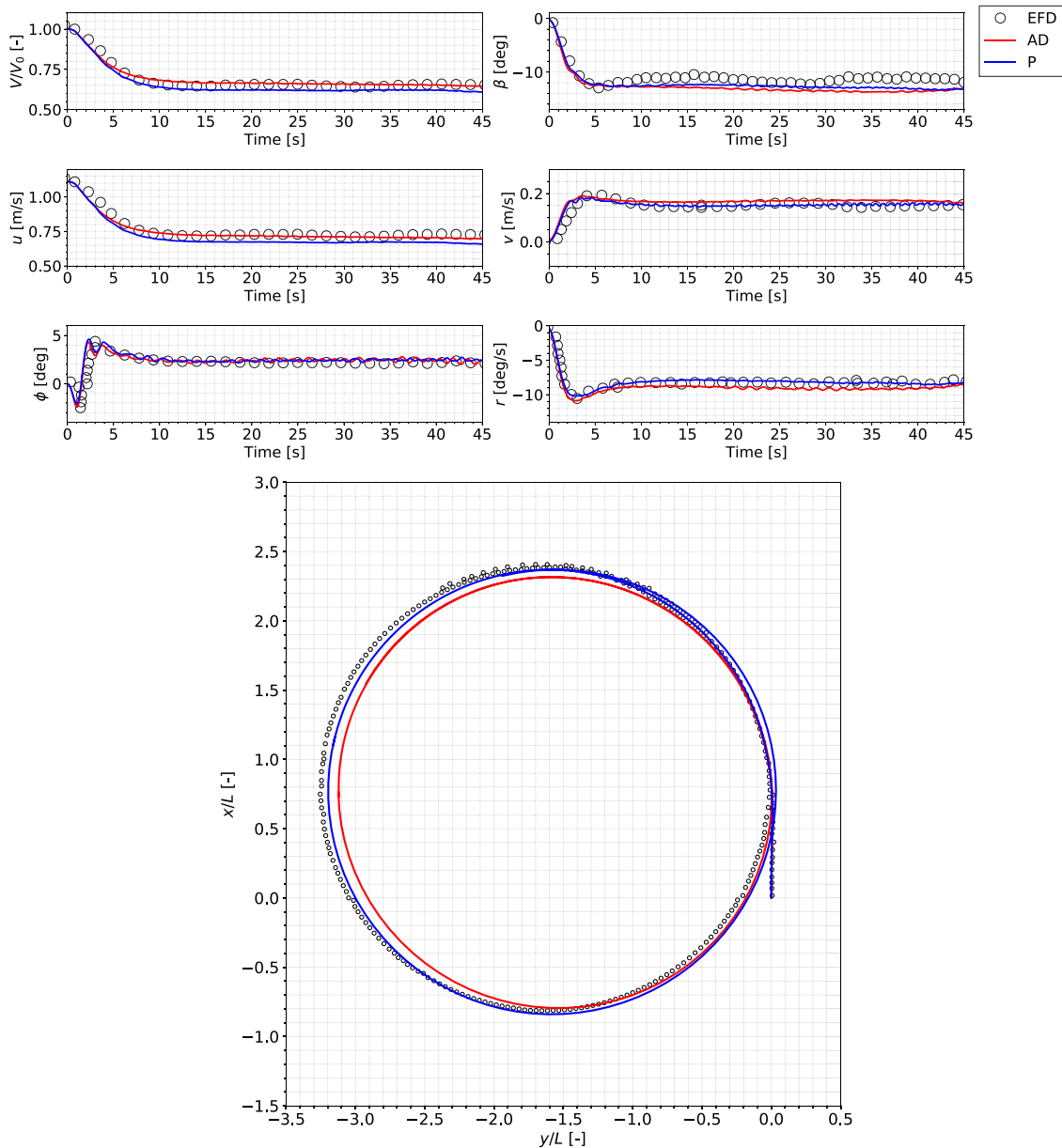


Fig. 7. Time histories of the ship velocities, motions, and trajectories during turning circle maneuver in calm water.

part of the turning maneuver (V_s/V_0), the AD method tends to overestimate it, suggesting a discrepancy in its representation of the ship's surge and sway velocity during the maneuver. This observation is supported by Fig. 7, particularly when the surge (u) and sway (v) velocities are examined. Generally in case of AD sway velocity is overestimated in steady part of the turn which is mainly due to the simplified propeller representation which does not account for the propeller's side force. The P method shows a slight underestimation of the forward velocity, indicating a more accurate approach in capturing velocity dynamics. Steady-state non-dimensional yaw rate ($r'_s = r_s \cdot L/V_s$) and drift angle (β_s) are generally larger in case of AD method compared to P method which implies better capability of the P method to predict yaw and sway motions during circle maneuver.

The results from AD and P propeller models generally align with the trends observed in EFD data. Overall, the analysis reveals the P method as generally more aligned with the EFD data, suggesting it is enhanced capability in replicating the complex aspects of ship maneuvering. A key factor contributing to the differences between the

P and AD models is the absence of propeller side force in the AD model. In maneuvering scenarios like a turning circle, the inflow to the propeller deviates significantly from the axial alignment, typical in straight-ahead conditions. This deviation introduces a notable component of force perpendicular to the propeller's axis of rotation, known as the side force. The side force plays a crucial role in maneuvering dynamics, particularly influencing the ship's sway velocity, yaw rate, and drift angle. When a ship is turning, the non-axial inflow leads to an increased side force, which, if not accurately accounted for, can significantly impact the ship's maneuvering characteristics. An overlooked or underestimated side force in simulations or calculations leads to an overestimation of the net side force and turning moment. This in turn manifests in larger sway velocity and yaw rate. Consequently, the increased sway velocity amplifies the drift angle, while reducing the ship's forward speed as depicted in Fig. 7. These observations align with observations from Aram and Mucha (2023) where they performed detailed analysis of different propeller models for a ship maneuvering in calm water.

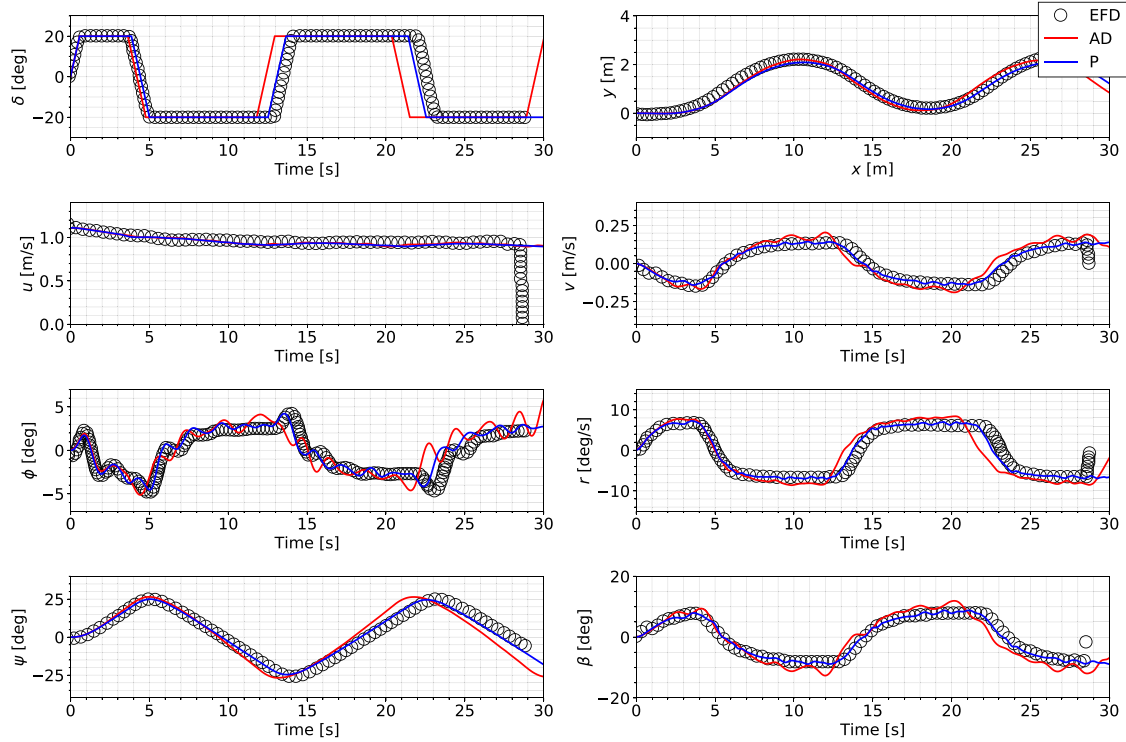


Fig. 8. Time histories of the ship velocities, motions, and trajectory during zig-zag 20/20 maneuver in calm water.

Overall, the discrepancies observed, particularly in drift angles and yaw rates, highlight the need for further refinement and calibration of both simulation methods to enhance accuracy.

4.4. Zig-zag 20/20 maneuver in calm water

Standard zig-zag maneuvering test can give insight into a ship's ability to control heading by steering from one side to the other. Analysis of the maneuver data can give insight into different aspects of the ship's dynamic response, such as its rudder effectiveness, yaw stability, and overall maneuverability under varying conditions. This test is crucial for evaluating the ship's steering performance and agility, crucial factors for safe and efficient navigation.

Simulation of a zig-zag 20/20 maneuver in calm water is started from the stable solution of a self-propulsion simulation for both AD and P method. Same as in case of turning circle maneuver simulation, propeller rotation rate is kept constant. During the simulation equations for 6-DOF are solved. Comparison of the zig-zag 20/20 parameters for AD and P methods is presented in Table 5. Calculated relative differences between CFD and EFD data are denoted in braces. Time histories of the ship velocities, motions, and trajectories are depicted in Fig. 8.

In the analysis of the zig-zag maneuver data, a comparison between the CFD simulations, both AD and P method, and the EFD data reveals a detailed picture of ship maneuverability. For the first overshoot angle, the AD model tends to overestimate by 14.16%, whereas the P model shows a more accurate representation with an underestimation of 11.98% compared to the EFD. This pattern is indicative of the P model's closer alignment with real-world dynamics in capturing the ship's initial response to rudder input. The time to reach the first overshoot angle shows a minor deviation in both CFD methods, with the AD model slightly overestimating (+2.5%) and the P model showing a notable underestimation (−8.48%). Further, the AD model considerably overestimates the maximum drift angle (1st Overshoot β_{\max}) by 28.83%, whereas the P model's overestimation is more modest at 3.97%. This trend continues with the second overshoot angle, where

Table 5

Zig-zag 20/20 calm water parameters.

	EFD	AD	P
1st overshoot angle, °	5.7	6.507 (+14.16%)	5.017 (−11.98%)
1st overshoot angle Time $\cdot V_0/L$, −	0.46	0.471 (+2.5%)	0.421 (−8.48%)
1st overshoot β_{\max} , °	7.4	9.533 (+28.83%)	7.694 (+3.97%)
1st overshoot ϕ_{\max} , °	4.7	5.277 (+12.27%)	4.547 (−3.26%)
1st overshoot $r_{\max} \cdot L/V_0$, −	0.34	0.381 (+12.15%)	0.342 (+0.57%)
2nd overshoot angle, °	4.9	6.760 (+37.96%)	4.637 (−5.37%)
2nd overshoot angle Time $\cdot V_0/L$, −	0.46	0.465 (+1.03%)	0.414 (−9.95%)
2nd overshoot β_{\max} , °	8.1	12.894 (+59.19%)	8.605 (+6.24%)
2nd overshoot ϕ_{\max} , °	4.4	4.182 (−4.96%)	4.226 (−3.94%)
2nd overshoot $r_{\max} \cdot L/V_0$, −	0.32	0.427 (+33.44%)	0.320 (0.00%)
Period $T \cdot V_0/L$, −	6.6	6.29 (−4.63%)	6.46 (−2.16%)

the AD model overestimates by a significant 37.96%, and the P model slightly underestimates by 5.37%. In terms of the time taken to reach the second overshoot angle, both models show a slight difference from EFD, with the AD model closely aligned (+1.03%) and the P model underestimating (−9.95%). This discrepancy may stem from the models' differing interpretations of the ship's dynamic response after the initial turn. The period to complete one zig-zag turn is underestimated by both models, with the AD model showing a deviation of −4.63% and the P model −2.16%.

Overall, while both CFD models provide a good approximation of zig-zag maneuver parameters, the P method generally aligns more closely with EFD data. The observed discrepancies between the EFD

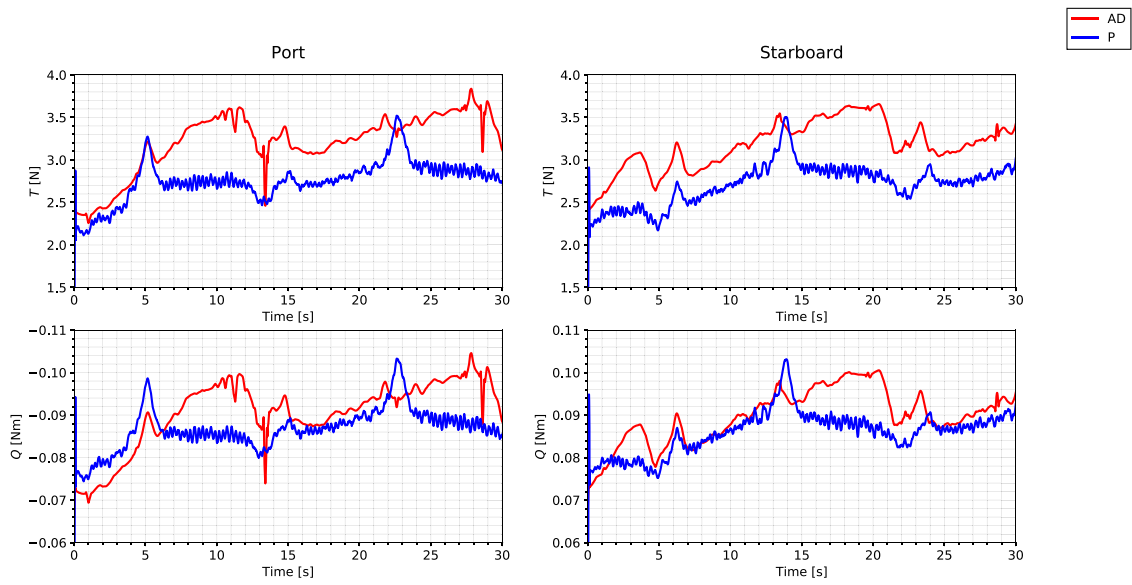


Fig. 9. Time histories of the propellers thrust and torque during zig-zag 20/20 maneuver in calm water.

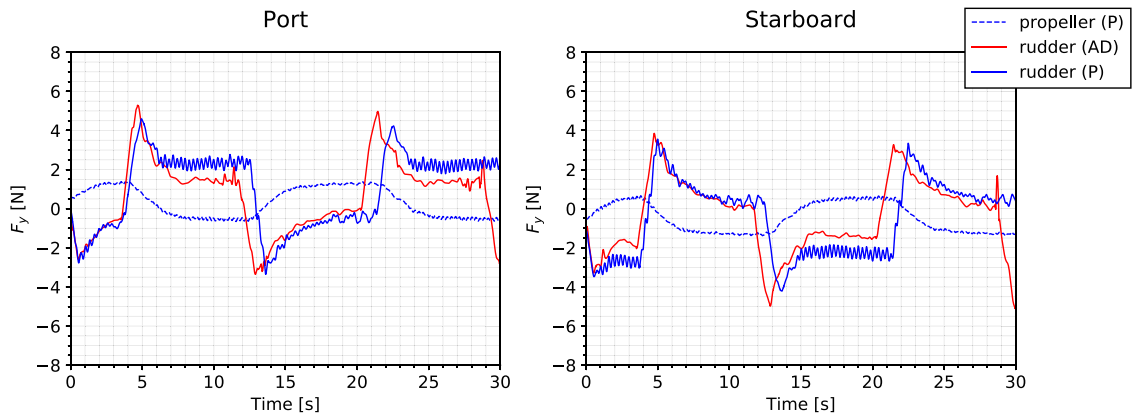


Fig. 10. Time histories of the propeller and rudder side force during zig-zag 20/20 maneuver in calm water.

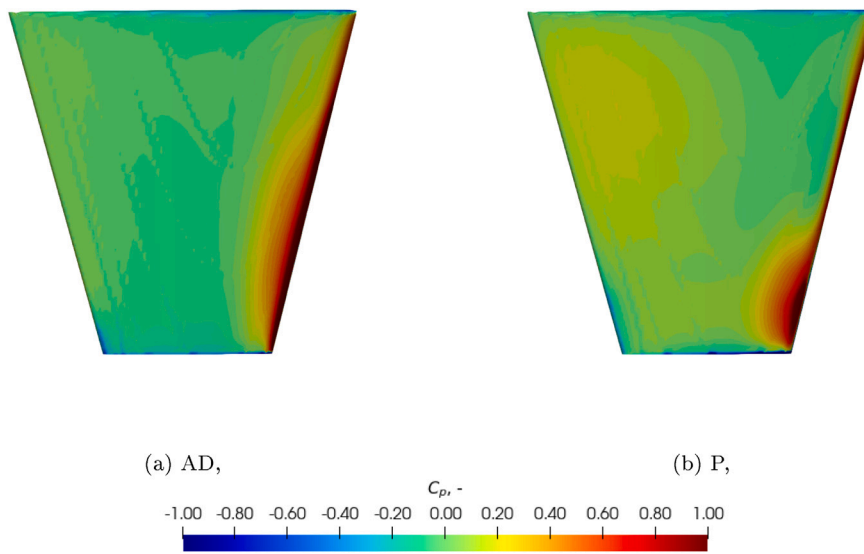


Fig. 11. Distribution of the pressure coefficient $C_p = (p_d / (0.5 \cdot \rho_w \cdot V^2))$ on the port rudder at neutral rudder angle.

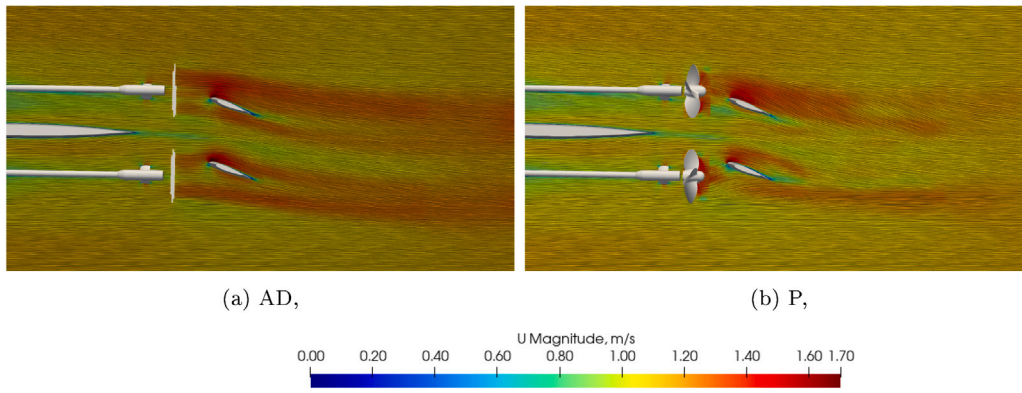


Fig. 12. Velocity magnitude contours along rudder mid-span plane at rudder maximum deflection angle instance (20°).

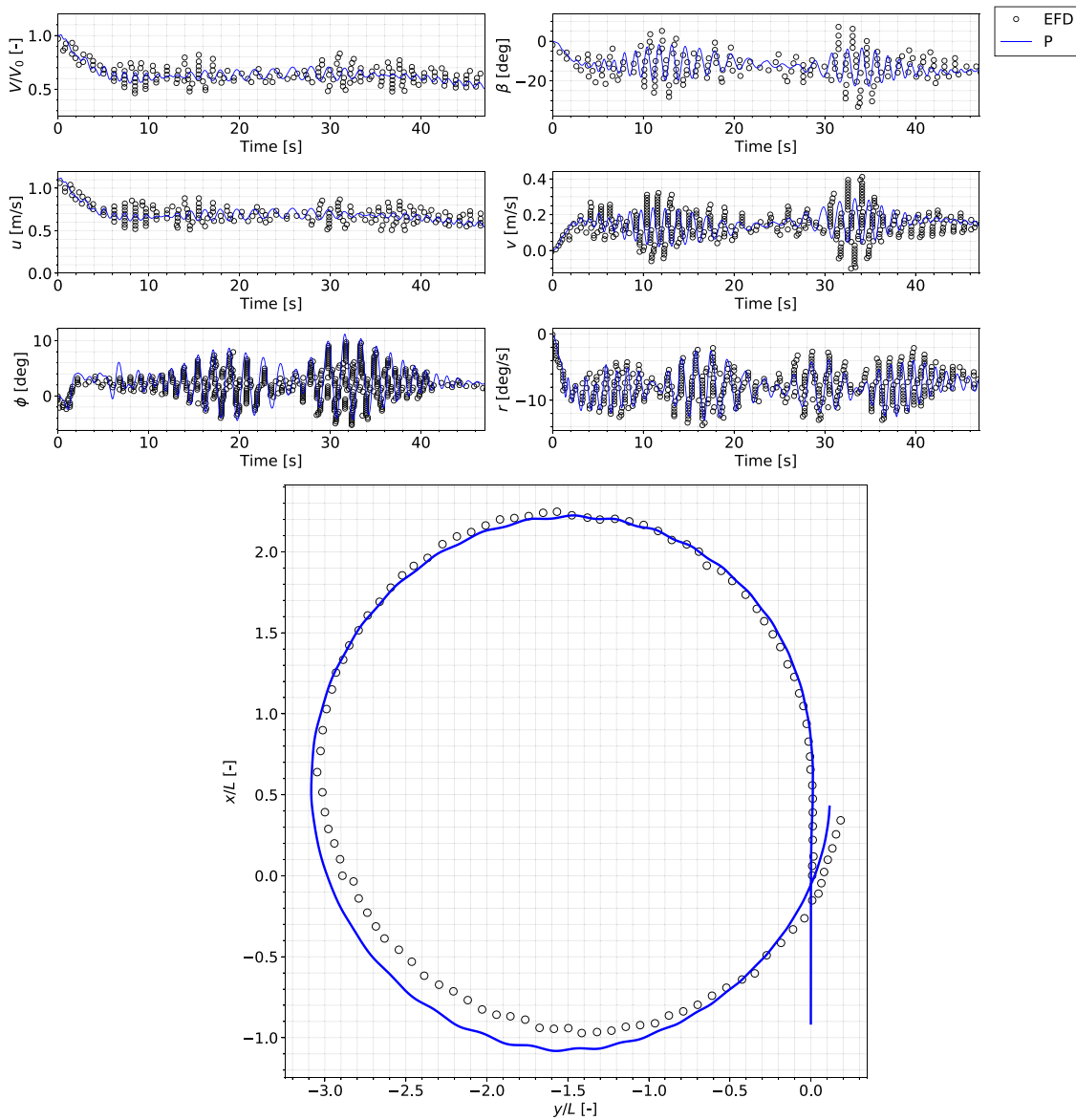


Fig. 13. Time histories of the ship velocities, motions, and trajectory during turning circle maneuver in waves ($\lambda = L$, $H/\lambda = 0.02$).

and the AD model are primarily due to the model's simplifications in representing the complex interactions between the hull, propeller, and rudder during the zig-zag maneuver. Fig. 9 depicts the time histories of thrust and torque for both the port and starboard propellers using

the AD and P methods. Due to its assumption of an infinite-bladed propeller and a uniform inflow velocity distribution, the AD model neglects the local character of inflow conditions. Consequently, this leads to differences in thrust and torque compared to the P method.

Despite the P method in this study using only 10% of the inertial propeller representation, the rotation and actual geometry of the propeller blades affect the accuracy of the predicted thrust and torque, thereby influencing simulation accuracy. Additionally, the P method accounts for propeller side force, unlike the AD method, as depicted in Fig. 10. The propeller side force, oriented opposite to the rudder side force, generates an additional yaw moment contributing to the overall moment balance. Furthermore, discrepancies in rudder side force between the AD and P methods are also evident. The simplified AD method induces a different flow field downstream of the propeller plane compared to the P method, as illustrated in Fig. 12. This variation in local flow fields affects pressure distribution on the rudders (Fig. 11) and consequently impacts force components.

The comparison of the AD and P models in the zig-zag maneuver simulations clearly shows the challenges in accurately mimicking ship maneuvers through computational methods. While both models offer valuable insights, this study highlights the need for careful adjustment and analysis of simulation methods and parameters to better reflect actual conditions. It becomes evident that a deeper understanding of how the ship's hull, propeller, and rudder interact is crucial for improving the precision of these simulations. This analysis points to the ongoing need to refine and improve simulation approaches, ensuring they remain effective for designing and assessing ship maneuverability in various scenarios.

4.5. Turning circle maneuver in head waves ($\lambda = L$, $H/\lambda = 0.02$)

In the analysis of turning circle maneuver in head waves characterized by wavelength $\lambda = L$ and wave steepness $H/\lambda = 0.02$, the P method is employed only. The outcomes of this simulation are important for comprehending the nuances of ship maneuverability during turning maneuver under specific wave conditions. This analysis is particularly significant as it follows after verifying the accuracy of the P method in calm water conditions, providing a basis for its application in waves. Obtained results are summarized in Table 6 accompanied with relative differences between CFD and EFD. Ship velocities, trajectory, and ship motions are depicted in Fig. 13. For the advance, the P simulation showed a 6.27% overestimation compared to EFD, indicating a slightly longer distance traveled by the ship to change its heading by 90 degrees in wave conditions. Tactical diameter and transfer values are closely matched with EFD, with deviations of 2.38% and -1.57% respectively, suggesting the model's effectiveness in capturing the lateral movement and turning ability of the ship in head waves. The steady turning diameter and the times to change heading are also accurately approximated by the P model. The most significant deviation is observed in $T_{90}V_0/L$ with a -1.76% underestimation, demonstrating the model's reliability in representing the ship's dynamic response throughout the turning maneuver under wave conditions. The ship's forward velocity is overestimated by 3.29%, which indicates slightly larger predicted sway velocity (Fig. 13), possibly influenced by wave interactions. Non-dimensional yaw rate and drift angle are underestimated by 8.71% and 7.66%, respectively. The roll angles, encompassing the minimum roll angle (ϕ_{min}), maximum roll angle (ϕ_{max}), and the steady-state roll angle (ϕ_s), display a generally good alignment with the experimental data. However, the maximum roll angle (ϕ_{max}) exhibits a more notable deviation, being overestimated by 31.30% in the simulations. The oscillatory response in sway velocity and yaw rate, observed in the simulations (Fig. 13), corresponds to the ship's encounter frequency with the waves and varies significantly with its orientation relative to wave direction. The oscillatory response tends to be minimal when the ship's heading aligns with head or following seas, suggesting a more stable maneuvering condition. In contrast, the oscillation intensifies when the ship faces beam seas or orientations close to it, indicating increased instability and a more pronounced effect of the waves on the ship's maneuverability. This pattern highlights

Table 6

Turning circle in waves parameters ($\lambda = L$, $H/\lambda = 0.02$).

	EFD	P
Advance, AD/L , -	2.085	2.216 (6.27%)
Tactical, TD/L , -	3.022	3.094 (2.38%)
Transfer, TR/L , -	1.218	1.199 (-1.57%)
Steady, D/L , -	3.208	3.187 (-0.63%)
$T_{90}V_0/L$, -	4.037	3.966 (-1.76%)
$T_{180}V_0/L$, -	7.888	7.977 (1.13%)
$T_{360}V_0/L$, -	16.085	15.881 (-1.26%)
V_s/V_0 , -	0.610	0.630 (3.29%)
r'_s , -	-0.691	-0.631 (-8.71%)
β_s , °	12.730	13.706 (7.66%)
ϕ_{min} , °	-2.314	-2.423 (-4.69%)
ϕ_{max} , °	4.622	6.068 (31.30%)
ϕ_s , °	2.768	2.903 (4.89%)

the impact of wave orientation on the dynamic behavior of the ship during maneuvers in waves.

In summary, the P method effectively simulates turning circle maneuver in regular head waves, with some discrepancies in certain key parameters. These results indicate the model's proficiency in capturing complex hydrodynamic interactions during ship maneuvering in waves, while also highlighting areas for further refinement.

4.6. Zig-zag 20/20 maneuver in waves ($\lambda = L$, $H/\lambda = 0.02$)

Similar to the turning circle maneuver, the zig-zag maneuver simulation in regular head waves, characterized by a wavelength of $\lambda = L$ and a wave steepness of $H/\lambda = 0.02$, employs only the P method. The simulation maintains a constant propeller rotation rate, as determined from the self-propulsion simulation, and utilizes a 6-DOF model. The resulting time histories of the ship's velocities, trajectory, and motions, captured during this simulation, are illustrated in Fig. 14.

The simulation results reveal that the P method closely mirrors the trends observed in the experimental data for all measured quantities. Similar to the calm water zig-zag maneuver, the time period required to complete a single zig-zag motion is slightly underestimated. The time histories of propeller thrust and torque, as presented in Fig. 15, are influenced by the combined effects of ship motions, rudder actions, and wave presence. Notably, fluctuations in thrust and torque are more pronounced under wave conditions compared to the calm water scenario. Furthermore, larger fluctuations in propeller and rudder side force, which follow a similar pattern to those observed in calm water simulations (Fig. 16), are evident. As with previous cases, the P method's capability to account for propeller side force resulting from non-axial inflow contributes to its more accurate alignment with experimental data.

5. Conclusion

This study has extensively explored the capabilities of Computational Fluid Dynamics (CFD) in simulating ship maneuvers under various conditions, focusing on a model-scale ONRT surface combatant. Employing both the actuator disc (AD) and partially rotating grid (P) methods, this research has yielded important insights into ship

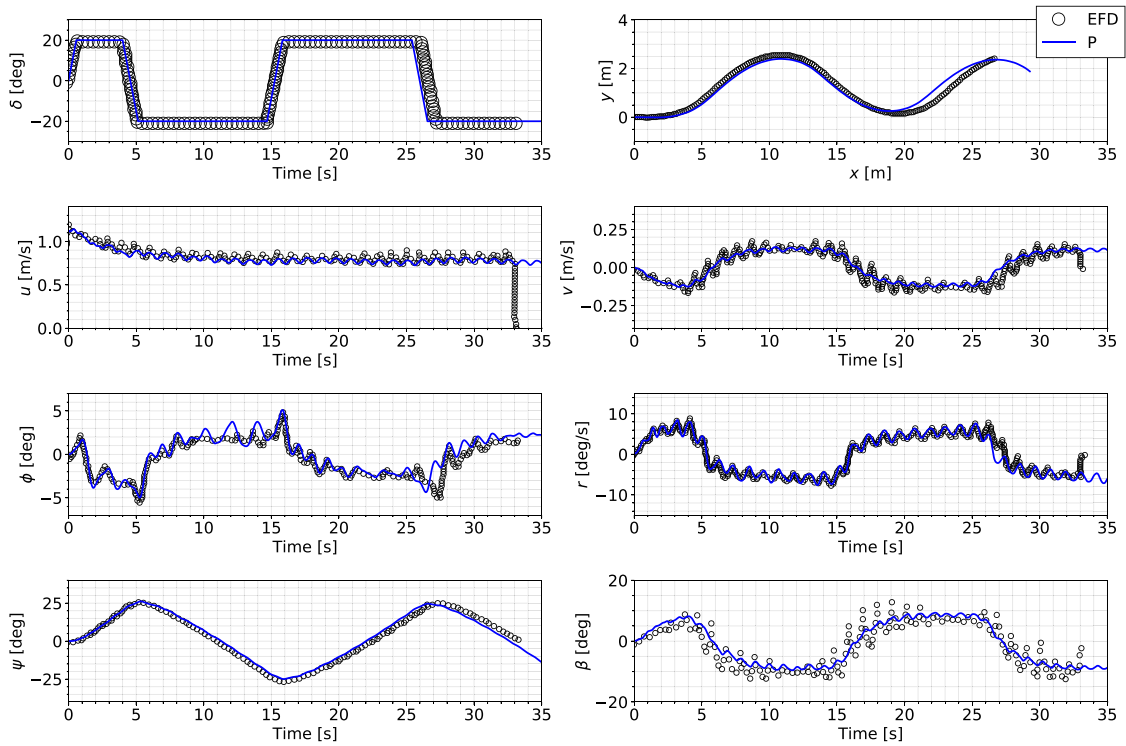


Fig. 14. Time histories of the ship velocities, motions, and trajectory during zig-zag 20/20 maneuver in waves ($\lambda = L$, $H/\lambda = 0.02$).

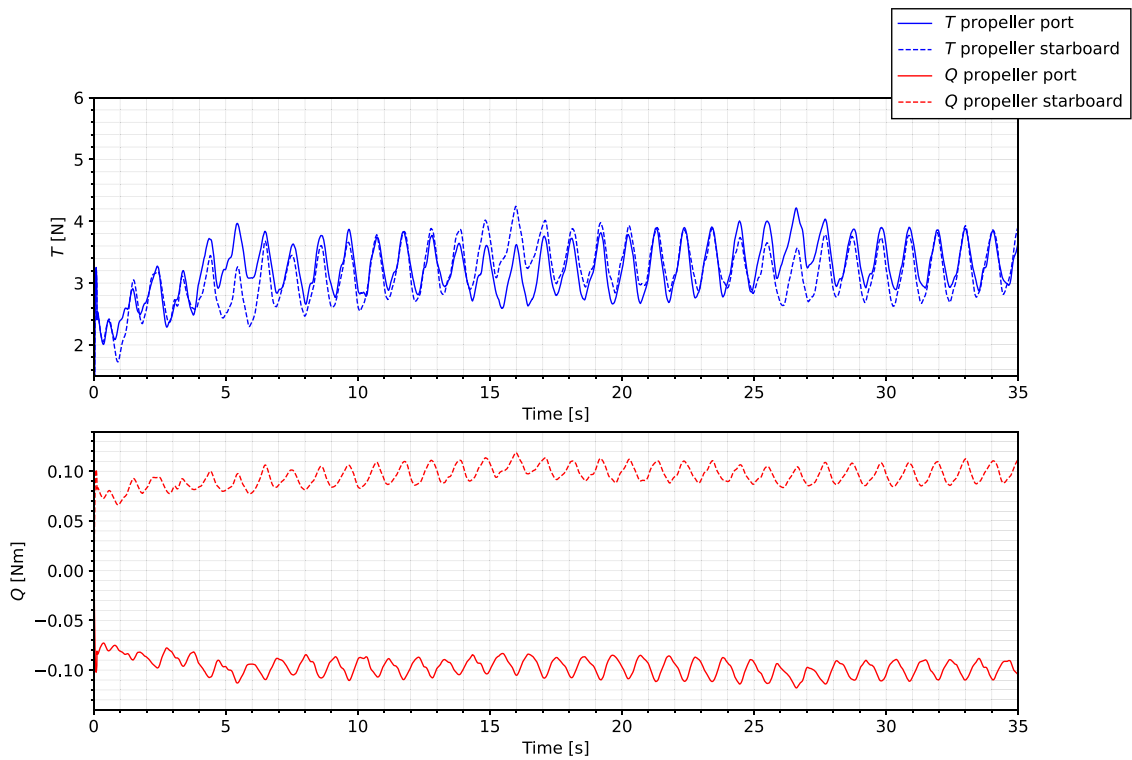


Fig. 15. Time histories of the propellers thrust and torque during zig-zag 20/20 maneuver in waves ($\lambda = L$, $H/\lambda = 0.02$).

maneuverability in calm and wave-affected waters. The conclusions drawn from this comprehensive analysis can be outlined as follows:

1. The propeller open water simulations, essential for obtaining necessary data for the AD model, indicated an overestimation in CFD results for thrust and torque coefficients at model scale,

particularly at higher advance ratios. This was attributed to the distinctive flow characteristics at model scale, such as laminar flow and pronounced flow separation.

2. In self-propulsion simulations, both the AD and P methods showed reasonable accuracy in estimating the propeller rotation rate. However, the small absolute values in experimental data for

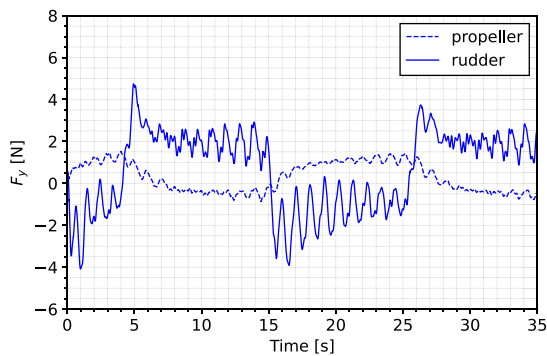


Fig. 16. Time histories of the propeller and rudder side force during zig-zag 20/20 maneuver in waves ($\lambda = L$, $H/\lambda = 0.02$).

sinkage and trim led to large relative discrepancies, emphasizing the need for nuanced interpretation of CFD results.

- Comparative analysis of calm water turning circle and zig-zag maneuvers revealed that the P method closely aligns with experimental data, effectively capturing ship velocities, trajectories, and dynamic responses. The study underscored the significance of accounting for propeller side force in maneuvering simulations, a factor overlooked in the AD model.
- Simulations of maneuvers in head waves demonstrated the P method's effectiveness in replicating complex hydrodynamic interactions. While there were discrepancies in certain parameters, the method showed capability in capturing the essence of ship maneuvering in waves.
- The study's findings, particularly the P method's closer alignment with experimental data in various maneuvering scenarios, point to the potential of CFD as a robust tool for simulating ship maneuvers. The results underscore the ongoing need to refine and improve simulation approaches, ensuring they remain effective for designing and assessing ship maneuverability in diverse scenarios.

CRedit authorship contribution statement

Sanjo Đurasević: Writing – review & editing, Writing – original draft, Visualization, Validation, Software, Methodology, Conceptualization. **Inno Gatin:** Visualization, Validation, Software, Methodology, Investigation, Formal analysis, Conceptualization. **Hrvoje Jasak:** Writing – review & editing, Supervision, Software, Resources, Project administration, Methodology, Conceptualization.

Declaration of competing interest

The authors declare that they have no known competing financial interests or personal relationships that could have appeared to influence the work reported in this paper.

References

Aram, S., Mucha, P., 2023. Computational fluid dynamics analysis of different propeller models for a ship maneuvering in calm water. *Ocean Eng.* 276 (December 2022), 114226. <http://dx.doi.org/10.1016/j.oceaneng.2023.114226>.

Brogliola, R., Dubbioso, G., Durante, D., A., Di Mascio, 2015. Turning ability analysis of a fully appended twin screw vessel by CFD. Part I: Single rudder configuration. *Ocean Eng.* (ISSN: 0029-8018) 105, 275–286. <http://dx.doi.org/10.1016/j.oceaneng.2015.06.031>, <https://www.sciencedirect.com/science/article/pii/S0029801815002747>.

Carrica, P.M., Ismail, F., Hyman, M., Bhushan, S., Stern, F., 2013. Turn and zigzag maneuvers of a surface combatant using a URANS approach with dynamic overset grids. *J. Mar. Sci. Technol. (Japan)* 18 (2), 166–181. <http://dx.doi.org/10.1007/s00773-012-0196-8>.

Carrica, P.M., Mofidi, A., Martin, E., 2015. Progress toward direct CFD simulation of manoeuvres in waves. In: *MARINE 2015 - Computational Methods in Marine Engineering VI*. pp. 327–338.

Dubbioso, G., Durante, D., DiMascio, A., Brogliola, R., 2016. Turning ability analysis of a fully appended twin screw vessel by CFD. Part II: Single vs. twin rudder configuration. *Ocean Eng.* 117, 259–271. <http://dx.doi.org/10.1016/j.oceaneng.2016.03.001>.

Elshiekh, H.A., 2014. Maneuvering characteristics in calm water and regular waves for ONR tumblehome. <http://dx.doi.org/10.17077/etd.8fia5blv>.

Gatin, I., Vukčević, V., Jasak, H., Lalović, I., 2018. Manoeuvring simulations using the overset grid technology in foam-extend. In: *32nd Symposium on Naval Hydrodynamics (August)*. p. 10.

Gatin, I., Vukčević, V., Jasak, H., Rusche, H., 2017. Enhanced coupling of solid body motion and fluid flow in finite volume framework. *Ocean Eng.* 143, 295–304. <http://dx.doi.org/10.1016/j.oceaneng.2017.08.009>, URL <https://www.sciencedirect.com/science/article/pii/S0029801817304614>.

Guo, H.P., Zou, Z.J., Liu, Y., Wang, F., 2018. Investigation on hull-propeller-rudder interaction by RANS simulation of captive model tests for a twin-screw ship. *Ocean Eng.* 162 (May), 259–273. <http://dx.doi.org/10.1016/j.oceaneng.2018.05.035>.

IMO, 2002. Standards for ship manoeuvrability. [https://www.wcdn.imo.org/localresources/en/KnowledgeCentre/IndexofMOResolutions/MSCResolutions/MS137\(76\).pdf](https://www.wcdn.imo.org/localresources/en/KnowledgeCentre/IndexofMOResolutions/MSCResolutions/MS137(76).pdf), [Online (Accessed 29 November 2023)].

IMO, 2014. Guidelines on the method of calculation of the attained energy efficiency design index (EEDI) for new ships. [https://www.wcdn.imo.org/localresources/en/OurWork/Environment/Documents/245\(66\).pdf](https://www.wcdn.imo.org/localresources/en/OurWork/Environment/Documents/245(66).pdf), [Online (Accessed 29 November 2023)].

Issa, R., 1986. Solution of the implicitly discretised fluid flow equations by operator-splitting. *J. Comput. Phys.* 62 (1), 40–65. [http://dx.doi.org/10.1016/0021-9991\(86\)90099-9](http://dx.doi.org/10.1016/0021-9991(86)90099-9), URL <https://www.sciencedirect.com/science/article/pii/0021999186900999>.

ITTC, 2021. International Towing Tank Conference (ITTC) (2021), Practical Guidelines for Ship Self-Propulsion CFD. <https://www.ittc.info/media/9765/75-03-03-01.pdf>, [Online (Accessed 3 January 2023)].

Jasak, H., Vukčević, V., Gatin, I., 2015. Numerical simulation of wave loading on static offshore structures. *Springer Tracts Mech. Eng.* 16, 95–105. http://dx.doi.org/10.1007/978-3-319-16202-7_9.

Jin, Y., Duffy, J., Chai, S., Magee, R. A., 2019. DTMB 5415M dynamic manoeuvres with URANS computation using body-force and discretised propeller models. *Ocean Eng.* (ISSN: 0029-8018) 182, 305–317. <http://dx.doi.org/10.1016/j.oceaneng.2019.04.036>, <https://www.sciencedirect.com/science/article/pii/S002980181930174X>.

Kim, I.T., Kim, C., Kim, S.H., Ko, D., Moon, S.H., Park, H., Kwon, J., Jin, B., 2021a. Estimation of the manoeuvrability of the KVLCC2 in calm water using free running simulation based on CFD. *Int. J. Naval Archit. Ocean Eng.* 13, 466–477. <http://dx.doi.org/10.1016/j.ijnaoe.2021.05.004>.

Kim, D., Song, S., Jeong, B., Tezdogan, T., 2021b. Numerical evaluation of a ship's manoeuvrability and course keeping control under various wave conditions using CFD. *Ocean Eng.* 237 (July), 109615. <http://dx.doi.org/10.1016/j.oceaneng.2021.109615>.

Kim, D., Song, S., Tezdogan, T., 2021c. Free running CFD simulations to investigate ship manoeuvrability in waves. *Ocean Eng.* 236 (July), 109567. <http://dx.doi.org/10.1016/j.oceaneng.2021.109567>.

Menter, F., Kuntz, M., Langtry, R., 2003. Turbulence, heat and mass transfer 4. In: K (Ed.), *Turbulence, Heat and Mass Transfer 4*. pp. 625–632.

Mofidi, A., Carrica, P.M., 2014. Simulations of zigzag maneuvers for a container ship with direct moving rudder and propeller. *Comput. & Fluids* 96, 191–203. <http://dx.doi.org/10.1016/j.compfluid.2014.03.017>.

Patankar, S., Spalding, D., 1972. A calculation procedure for heat, mass and momentum transfer in three-dimensional parabolic flows. *Int. J. Heat Mass Transfer* 15 (10), 1787–1806. [http://dx.doi.org/10.1016/0017-9310\(72\)90054-3](http://dx.doi.org/10.1016/0017-9310(72)90054-3), URL <https://www.sciencedirect.com/science/article/pii/0017931072900543>.

Sanada, Y., Elshiekh, H., Toda, Y., Stern, F., 2019. ONR Tumblehome course keeping and maneuvering in calm water and waves. *J. Mar. Sci. Technol. (Japan)* 24 (3), 948–967. <http://dx.doi.org/10.1007/s00773-018-0598-3>.

Shang, H., Zhan, C., Liu, Z., 2021. Numerical simulation of ship maneuvers through self-propulsion. *J. Mar. Sci. Eng.* (ISSN: 2077-1312) 9 (9), <http://dx.doi.org/10.3390/jmse9091017>, <https://www.mdpi.com/2077-1312/9/9/1017>.

Tokyo, 2015. A workshop on CFD in ship hydrodynamics. https://t2015.nmri.go.jp/onrt_gc.html, [Online (Accessed 1 December 2023)] (2015).

Đurasević, S., Gatin, I., Uroić, T., Jasak, H., 2022. Numerical analysis of self-propulsion flow characteristics in model scale. *Ocean Eng.* 259, 111885. <http://dx.doi.org/10.1016/j.oceaneng.2022.111885>, URL <https://www.sciencedirect.com/science/article/pii/S0029801822012252>.

Đurasević, Sanjo, Gatin, Inno, Uroić, Tessa, Jasak, Hrvoje, 2022. Partially rotating grid method for self-propulsion calculations with a double body ship model. *Ocean Eng.* (ISSN: 0029-8018) 266, 113105. <http://dx.doi.org/10.1016/j.oceaneng.2022.113105>, <https://www.sciencedirect.com/science/article/pii/S0029801822023885>.

Đurasević, S., Gatin, I., Uroić, T., Jasak, H., 2023. Hydrodynamic performance of a full-scale ship with a Pre-Swirl Duct: A numerical study with partially rotating grid method. *Ocean Eng.* (ISSN: 0029-8018) 283, 115049. <http://dx.doi.org/10.1016/j.oceaneng.2023.115049>, <https://www.sciencedirect.com/science/article/pii/S0029801823014336>.

- Vukčević, V., Jasak, H., 2014. A conservative level set method for interface capturing in two-phase flows. In: 11th World Congress on Computational Mechanics; 5th European Conference on Computational Mechanics; 6th European Conference on Computational Fluid Dynamics. Vol. 2, pp. 1082–1095.
- Vukčević, V., Jasak, H., Gatin, I., 2017. Implementation of the Ghost Fluid Method for free surface flows in polyhedral Finite Volume framework. *Comput. & Fluids* 153, 1–19. <http://dx.doi.org/10.1016/j.compfluid.2017.05.003>.
- Vukčević, V., Jasak, H., Malenica, Š., 2016a. Decomposition model for naval hydrodynamic applications, Part I: Computational method. *Ocean Eng.* 121, 37–46.
- Vukčević, V., Jasak, H., Malenica, Š., 2016b. Decomposition model for naval hydrodynamic applications, Part II: Verification and validation. *Ocean Eng.* 121, 76–88. <http://dx.doi.org/10.1016/j.oceaneng.2016.05.021>.
- Wang, J., Wan, D., 2020. CFD study of ship stopping maneuver by overset grid technique. *Ocean Eng.* 197 (December 2019), 106895. <http://dx.doi.org/10.1016/j.oceaneng.2019.106895>.
- Wang, J., Zou, L., Wan, D., 2018. Numerical simulations of zigzag maneuver of free running ship in waves by RANS-Overset grid method. *Ocean Eng.* (ISSN: 0029-8018) 162, 55–79. <http://dx.doi.org/10.1016/j.oceaneng.2018.05.021>, <https://www.sciencedirect.com/science/article/pii/S0029801818307868>.
- Weller, H.G., Tabor, G., Jasak, H., Fureby, C., 1998. A tensorial approach to computational continuum mechanics using object oriented techniques. *Comput. Phys.* 12, 620–631.